Journal of Colloid and Interface Science 551 (2019) 47–60

Contents lists available at ScienceDirect

Journal of Colloid and Interface Science

journal homepage: www.elsevier.com/locate/jcis

Myristic acid based imidazoline derivative as effective corrosion inhibitor for steel in 15% HCl medium

Moses M. Solomon [a,*], Saviour A. Umoren [a], Mumtaz A. Quraishi [a], Mohammad Salman [b]

[a] Center of Research Excellence in Corrosion, Research Institute, King Fahd University of Petroleum and Minerals, Dhahran 31261, Saudi Arabia
[b] Department of Chemistry, Indian Institute of Chemistry, BHU, Varanasi 221005, India

GRAPHICAL ABSTRACT

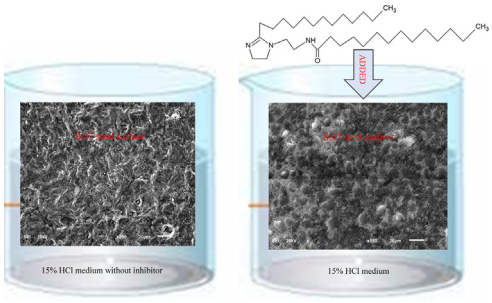

ARTICLE INFO

Article history:
Received 8 December 2018
Revised 14 April 2019
Accepted 1 May 2019
Available online 2 May 2019

Keywords:
Synthesis
Imidazoline
Acid corrosion
Corrosion inhibition
Steel
Performance

ABSTRACT

There is a high demand of effective and eco-friendly corrosion inhibitor for industrial applications. In an attempt to prepare a benign and effective corrosion inhibitor for acidizing purpose, an imidazoline derivative, N-(2-(2-tridecyl-4,5-dihydro-1H-imidazol-1-yl)ethyl)tetradecanamide (NTETD) was synthesized from myristic acid and diethyleneamine. The characterization of the newly synthesized compound was done using ^{1}H NMR, FTIR, and elemental analysis techniques. NTETD was examined as a corrosion inhibitor for low carbon steel in 15% HCl solution using weight loss, electrochemical impedance spectroscopy (EIS), potentiodynamic polarization (PDP), linear polarization (LPR), scanning electron microscope (SEM), energy dispersive spectroscopy (EDAX), atomic force spectroscopy (AFM), and X-ray photoelectron spectroscopy (XPS) techniques. It was found that, the optimum concentration of NTETD is 300 mg/L. With this concentration, inhibition efficiency above 93% is achievable. Results from PDP show that, NTETD acted as a mixed type corrosion inhibitor but with principal effect on cathodic corrosion half reactions. The calculated value of the adsorption-desorption equilibrium constant (1.015×10^3) reveals a strong bonding between NTETD molecules and the steel surface. The EDAX, FTIR, and XPS results confirm the adsorption of NTETD molecules on the steel surface. SEM and AFM results agree with experimental findings that NTETD is effective in corrosion mitigation of steel in 15% HCl solution. The possible corrosion inhibition mechanism by NTETD has been proposed.

1. Introduction

The demand for corrosion inhibitors for application in acidizing environment is on the increase. Oil well acidizing is a common industrial practice deployed for the enhancement of hydrocarbons

* Corresponding author.
E-mail address: moses.solomon@kfupm.edu.sa (M.M. Solomon).

https://doi.org/10.1016/j.jcis.2019.05.004
0021-9797/

production or recovery of hydrocarbons from depleted wells. In this practice, hydrochloric acid solution in the concentration range of 15–32% (depending on whether the formation rock is made of sandstone or limestone) is force down a well bore to etch the formation rocks and create larger flow channels [1–4]. As it is known, HCl is corrosive hence corrosion of oil well metallic structures is inevitable. Normally, corrosion inhibitor is added to the acid solution as a measure of controlling the corrosion of metallic structures. Common corrosion inhibitors for the oil and gas applications are organic compounds from the family of amides, imidazolines, nitrogen quaternaries, polyoxyalkylated amines, salts of nitrogenous molecules with carboxylic acids, or nitrogen heterocyclics [5–7]. Unfortunately, some of the common corrosion inhibitors fail in acidizing environment because of the severity of the environment [8].

Imidazoline represents an interesting class of organic compounds having three isomeric forms: 2-imidazoline (Fig. 1(a)), 3-imidazoline (Fig. 1(b)), and 4-imidazoline (Fig. 1(c)). The 2-imidazoline isomer is the most common and its ring is found in some natural products and pharmaceuticals [9,10]; its application as antihyperglycemic, anti-inflammatory, antihypertensive, antihypercholesterolemic, and antidepressant reagent has been documented [9,10]. For application as anticorrosive agent, the sensitivity of imidazolines to hydrolysis has been the limiting factor [11,12]. It had been found that the hydrolysis of imidazoline gives rise to products with little or no anticorrosion property [11,12]. Nevertheless, it has been established that the partitioning cum inhibiting properties of imidazoline in aqueous medium can be improved by introduction of suitable pendant group(s) [12]. The length of the pendant group and the position of attachment on the imidazoline ring are essential as they have remarkable influence on inhibition efficiency. For example, it was reported by Ramachandran et al. [13], that imidazoline compounds with substituent chain length of C < 12 exhibited poor inhibition towards iron corrosion. On the position of the substituent, Blair et al. [14] in the US patent 2,466,517 pointed out that, the most effective imidazoline inhibitors are those with long chain substituent attached on one of the nitrogen atoms of the imidazoline ring or on a relatively small organic radical attached to one of the nitrogen atoms of the ring.

There are quite a reasonable number of research information on imidazoline derivatives as metals corrosion inhibitor in sweet environment [15–18] but such information is very scanty [19–21] in acidic environment. In the few research publications on imidazoline derivatives as inhibitor in acidic environment, the organic compounds were found to be very effective. For example, He et al. [20] observed that 2-phenyl-2-imidazoline performed better than imidazole as inhibitor for AA5052 alloy in 1 M HCl solution. It was found that 5.2 mM of 2-phenyl-2-imidazoline achieved inhibition efficiency of 84.0% compared to 64.7% afforded by imidazole. In a more aggressive acid solution (15% HCl), Yadav et al. [21] reported that 150 ppm of 1-(2-aminoethyl)-2-oleylimidazoline and 1-(2-oleylamidoethyl)-2-oleylimidazoline afforded inhibition efficiency of 90.26% and 96.23%, respectively at 298 K for N80 steel. Recently, it was reported [22] that, a palmitic imidazoline compound, N-(2-(2-pentadecyl-4,5-dihydro-1H-imidazol-1-yl)ethyl)palmitamide (NIMP) exhibited outstanding corrosion inhibition effect towards N80 steel in 15% HCl solution at low and elevated temperatures. At optimum concentration (300 ppm), NIMP protected the steel surface by 97.92% and 95.59% at 25 °C and 60 °C respectively.

In this communication, we presents NTETD (Fig. 1(d)) as a potent corrosion inhibitor for steel in 15% HCl environment. In NTETD, the pendant group has 13 carbon atoms and is attached on a small group linked to the imidazoline moiety on one of the nitrogen atoms. NTETD therefore fits the perfect description of an effective corrosion inhibitor given by Ramachandran *et. al.* [13] and Blair et al. [14].

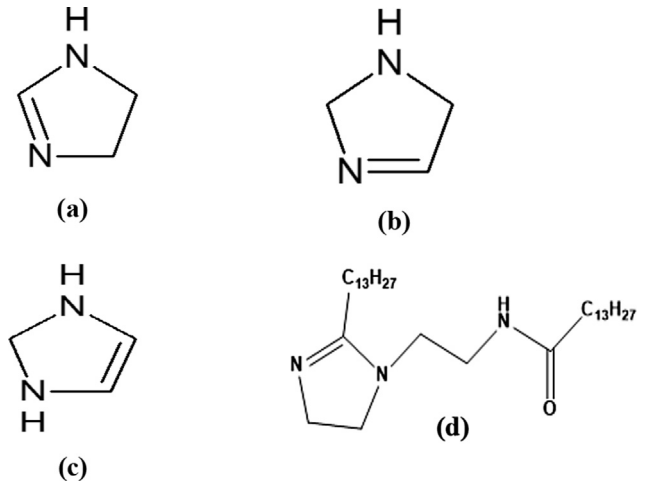

Fig. 1. Chemical structure of (a) 2-imidazoline, (b) 3-imidazoline, (c) 4-imidazoline, and (d) N-(2-(2-tridecyl-4,5-dihydro-1H-imidazol-1-yl)ethyl)tetradecanamide.

2. Experimental part

2.1. Chemicals used

The chemicals used for the synthesis of NTETD and in corrosion studies were procured from Merck, USA and include diethylenediamine (99%), myristic acid (≥99%), calcium oxide (≥99.99%), ethyl acetate (99.8%), and HCl (37%).

2.2. Synthesis of NTETD

We used a synthesis route similar to the one earlier reported by Bajpai and Tyagi [23]. Diethylenediamine (2.06 g), Myristic acid (9.8 g), calcium oxide (20 g) were accurately measured into an open Pyrex vessel (500 mL) and were carefully mixed. The reaction mixture was irradiated in a microwave oven for about 7 min utilizing a power of 850 W. The reaction mixture was left to cool to room temperature. Thereafter, 80 mL of ethyl acetate was introduced into the mixture and then heated until boiling. It was filtered while hot and the filtrate concentrated to dryness under vacuum. The white to yellowish NTETD (81% yield; melting point 54.4 °C) was obtained. The synthesis pathway is shown in Scheme 1.

2.3. Characterization of NTETD

The characterization of NTETD was achieved with an FTIR (PerkinElmer Version 10.03.05 instrument) spectrometer and a Bruker 500 MHz instrument operating at 500 MHz (^{1}H NMR characterization).

2.4. Anticorrosion studies

2.4.1. Materials/solutions preparation

Erdemir Steel Co., Turkey supplied the St37-2 steel sheet from which experimental samples were fabricated. The metal has the chemical composition as stated in our previous article [24]. Specimens of 3 × 3 cm (surface area = 9 cm^2) for gravimetric studies and circular-like shape samples with surface area of 0.79 cm^2 for electrochemical studies were mechanically cut from the metal sheet.

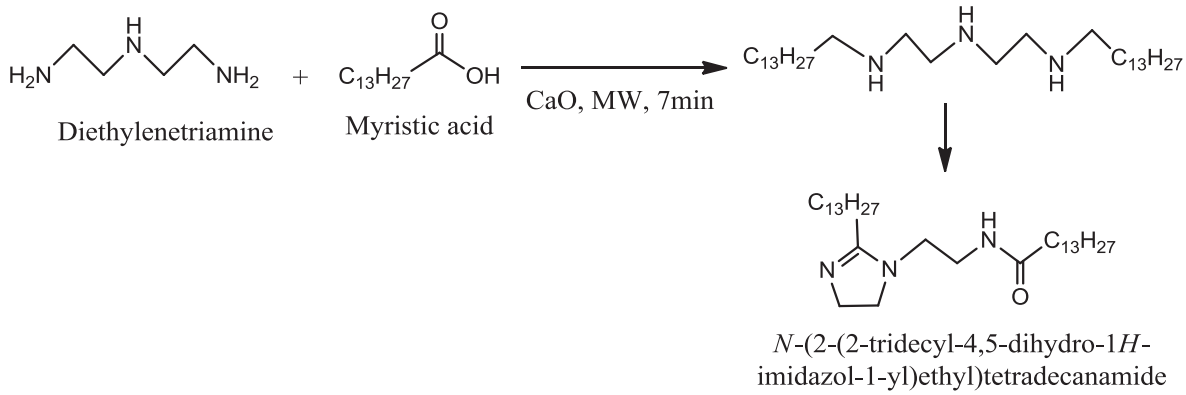

Scheme 1. Synthesis route of NTETD.

The specimens were subjected to mechanical abrasion using various grits of silicon carbide paper (#120 – #800). The dust generated by the abrasion process was removed by sonication in ethanol bath for 10 min. After this, the samples were degreased with C_2H_5OH and acetone, and then dried using sample drier [24]. The corrosive medium was 15% HCl solution and was prepared by diluting 37% HCl with distilled water. The concentration of NTETD studied was 50, 100, 200, 300, and 400 mg/L.

2.4.2. Weight loss experiments

The weight loss studies were performed in compliance with the ASTM standard procedure [25]. First, the initial weight of the prepared St37-2 steel samples, designated as W_0, was measured using a digital weighing balance of precision ±0.1 mg. Second, six (6) 150 mL reaction bottles labeled as bank, 50 mg/L, 100 mg/L, 200 mg/L, 300 mg/L, and 400 mg/L were filled with 100 mL of the respective solutions. Third, two pre-weighed coupons, with the help of a thread, were freely suspended in each of the reaction bottles. The bottles were placed in a thermostatic water bath maintained at 25 °C for 6 h. Fourth, at the expiration of 6 h, the corroded samples were retrieved, immersed in 1 M HCl for 20 s to loosen the corrosion products [26], washed thoroughly in running water and distilled water, rinsed in acetone, and finally dried in a stream of warm air. The dried metal specimens were reweighed and this weight was designated as W_1. The weight loss (WL) was calculated thus:

$$WL(g) = W_0 - W_1 \quad (1)$$

To compute the corrosion rate (v), the mean weight loss ($\bar{WL}$, mg) was used following Eq. (2) [16]:

$$v(\text{mm per year}) = \frac{87.6 \times \bar{WL}}{\rho AT} \quad (2)$$

where ρ = density of the steel sample (g cm^{-3}), A = surface area of the specimen (cm^2), and T = immersion time (h). The inhibition efficiency (η, %) of NTETD was calculated using Eq. (3):

$$\eta(\%) = \frac{v_{(\text{blank})} - v_{(\text{inh.})}}{v_{(\text{blank})}} \times 100 \quad (3)$$

where $v_{(\text{blank})}$ and $v_{(\text{inh.})}$ are the corrosion rates in the absence and presence of NTETD respectively.

2.4.3. Electrochemical measurements

The ASTM G3-89 [27] and G5-94 [28] standards were adopted in the conduct of the electrochemical experiments. An electrochemical instrument, Gamry Potentiostat/galvanost/ZRA (Ref 600) which has EIS300 and DC105 for impedance and polarization measurements respectively was utilized for the electrochemical studies. The electrochemical cell was a conventional three electrode system consisting of a graphite rod as the counter electrode, steel specimen as the working electrode, and silver/silver chloride as the reference electrode. Before kick starting electrochemical measurements, the working electrode was immersed in test solution for one hour and this was to establish at least a pseudo steady-state open-circuit potential (OCP) since genuine steady condition is practically impossible. For impedance recordings, the frequency was set at 100, 000 Hz to 0.01 Hz with amplitude of 10 mV peak to peak. For PDP measurements, the scanning of the sample electrode was done at a rate of 0.2 mV s^{-1} relative to free corrosion potential (E_{corr}) beginning from cathodic potential of −250 mV to anodic potential of +250 mV. An extrapolation method was used to get polarization parameters such as E_{corr}, current density (i_{corr}), anodic and cathodic Tafel slopes (β_a & β_c), *etc.* from the obtained polarization curves. For the analysis of impedance curves, Gamry Echem Analyst version 6.01 was used. Linear polarization resistance (LPR) measurements were achieved by polarizing the St37-2 steel electrode from −10 mV to +10 mV versus OCP at a sweep rate of 0.125 mV/s. The polarization resistance (R_p) was obtained from the slope of the potential-current graph in the vicinity of E_{corr}.

2.4.4. Surface examination

The surface morphologies of St37-2 samples exposed to 15% HCl environments in the absence and presence of NTETD for 24 h and the elemental composition of the corrosion products and/or adsorbed NTETD films on the sample surfaces were determined with the help of a Scanning Electron Microscope (SEM) JEOL JSM-6610 LV coupled to EDAX. The acceleration voltage of SEM instrument was 20 kV. The instrument, 5420 atomic force microscope (N9498S, Agilent Technologies, UK) operated in the contact mode under normal conditions was utilized to assess the roughness characteristics of the studied metal surfaces. A ESCALAB 250Xi XPS spectrometer with a monochromatic Al Kα X-ray source was used for XPS analysis. The data were obtained from the sample surface directly without Ar ion sputtering. Analysis of the XPS data was done using Avantage v5,51,0,5371 software. Meanwhile, the preparation procedure of samples for SEM-EDAX, XPS, and AFM analysis was different. For AFM analysis, the specimens after removing from test solutions were gently washed with distilled water, rinsed with acetone, and dried using sample drier before subjecting to the analysis. The cleaning process was avoided in samples used for SEM, EDAX, and XPS analysis; reason being that, our interest was on the adsorbed film.

3. Results and discussion

3.1. Chemical synthesis

The successful synthesis of NTETD from diethylenediamine and Myristic acid (Scheme 1) was confirmed via ^{1}H NMR and FTIR analysis. The ^{1}H NMR and FTIR spectra obtained for the synthesized imidazoline compound are presented in Fig. 2. In Fig. 2(a), the basic characteristic peaks of NTETD can be clearly seen. For instance, the chemical shift from the methylene protons that linked Myristic acid component to imidazolium ring can be seen at 2.46 ppm. The chemical shifts emanating from the methylene proton next to the carbonyl group (–CONH) is seen at 2.10 ppm. Also, the chemical shifts from the imidazoline ring protons appears at 3.00 and 4.00 ppm. In the FTIR spectrum (Fig. 2(b)), the imidazoline ring N—H stretching band is obvious at 2849 cm^{-1} and the characteristic peak of amide C=O stretching is noted at 1641 cm^{-1}.

3.2. Anticorrosion studies

3.2.1. OCP studies

The variation of the open circuit potential of working electrode with immersion duration in the studied electrolyte devoid of and containing different concentrations of NTETD is shown in Fig. 3. In the free acid solution, the initial open circuit potential of the electrode was −551.1 mV vs. Ag/AgCl. Similarly, in acid solutions containing 50, 100, 200, 300, and 400 mg/L NTETD, the initial open circuit potential of −522.3, −512.2, −529.7, −532.3, and

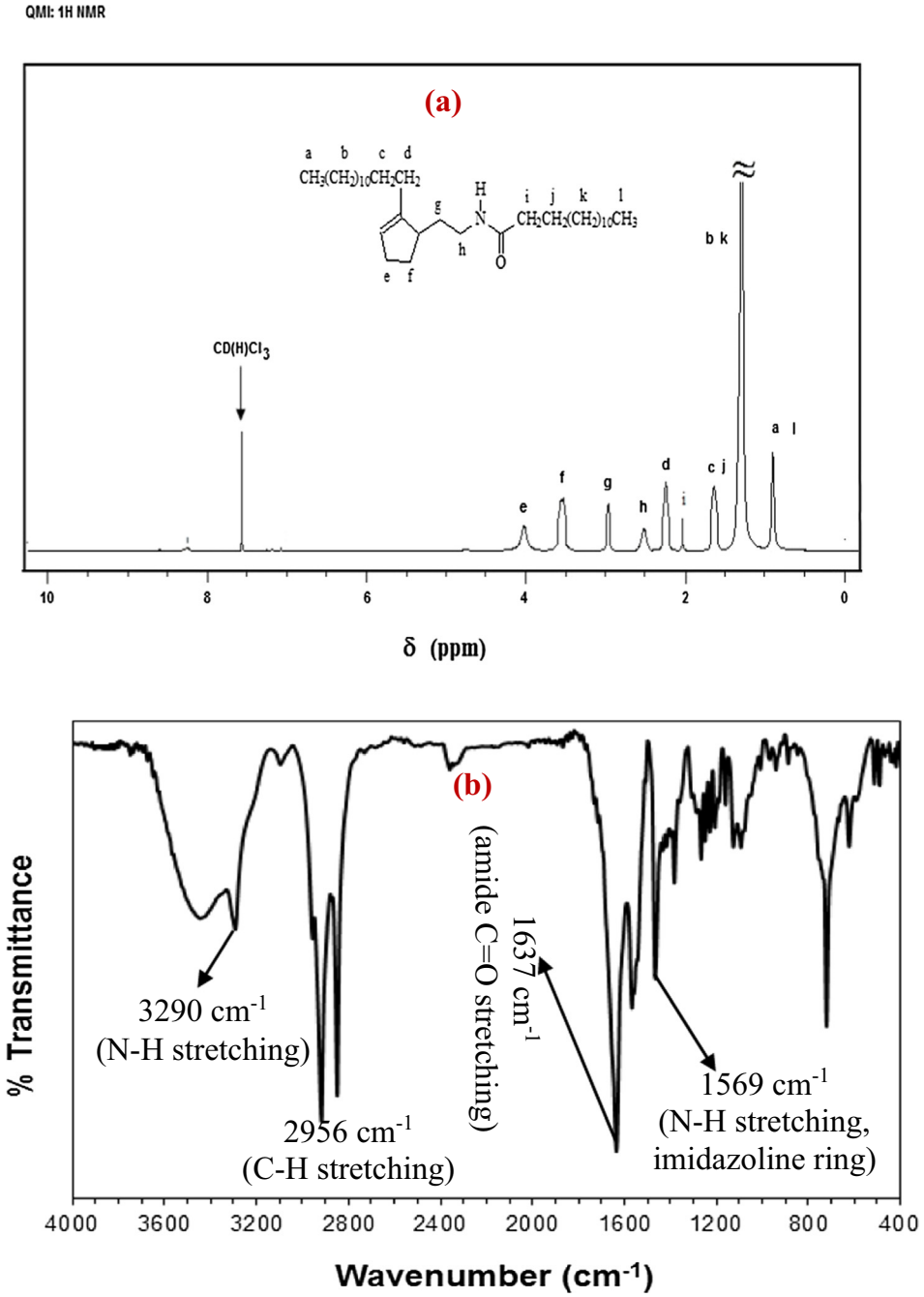

Fig. 2. (a) ^{1}H NMR and (b) FTIR spectra of N-(2-(2-tridecyl-4,5-dihydro-1H-imidazol-1-yl)ethyl)tetradecanamide.

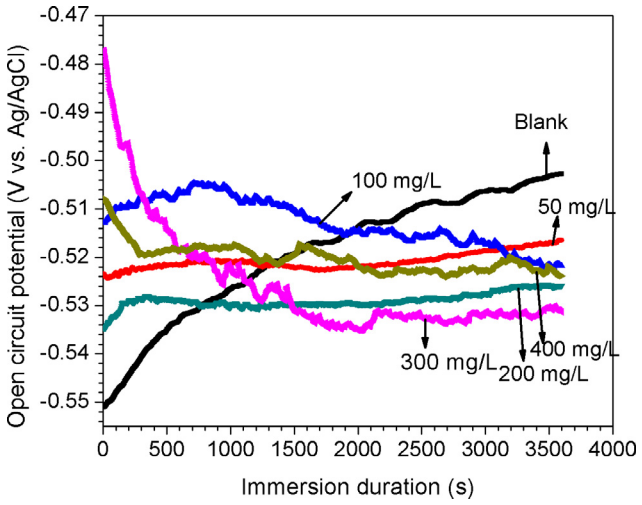

Fig. 3. Open circuit potential variations with time for St37–2 steel in 15% HCl solution without and with different concentrations of N-(2-(2-tridecyl-4,5-dihydro-1H-imidazol-1-yl)ethyl)tetradecanamide at 25 °C.

−517.8 mV vs. Ag/AgCl respectively was recorded. The initial open potential recorded in the inhibited systems is nobler compared to that recorded in free acid solution. It could be observed from the figure that the open circuit potential for the blank solution increases with immersion time before attaining pseudo-stability at about 1600 s, while that of the inhibited solutions decreases. The observed changes in open circuit potential could be associated with the adsorption of inhibitor molecules on the electrode surface [29]. Organic inhibitors can retard metals corrosion by intercepting anodic or cathodic corrosion reactions or both [29,30]. The displacement of open circuit potential in inhibited system relative to uninhibited can be used as a basis for inhibitor categorization [30–32]. Generally, a significant displacement is required and the benchmark is put at ±85 mV [30–32]. In our case, the difference between the initial open circuit potential recorded in free acid solution and 50, 100, 200, 300, and 400 mg/L NTETD inhibited systems is 28, 40, 18, 74, and 44 mV vs. Ag/AgCl respectively. Going by these values, it is justifiable to claim that NTETD demonstrated principal corrosion inhibitory effect on the cathodic half reactions.

3.2.2. EIS studies

Fig. 4(a) shows the Nyquist representative impedance for low carbon steel sample in studied corrodent free from and containing various dosages of NTETD at 25 °C. At high frequency range, irregular semicircles are seen and is common when corrosion process is controlled by charge transfer [33,34]. Additionally, in the inhibited impedance graphs, small and unresolved semicircle is observed at low frequency region. This could arise due to the double layer structure of adsorbed NTETD molecules on the electrode surface [35–37]. The imperfectness of the semicircles is a common feature of solid electrodes and factors such as micro roughness and heterogeneity of working electrode [35,38] as well as substance transmission actions [39] could be responsible. The corrosion inhibiting influence of NTETD could be clearly seen in the figure. For instance, the size of the Nyquist impedance of the protected systems is bigger than that of unprotected system. It means that the charge transfer process was resisted in the inhibited systems probably due to the adsorption of inhibitor molecules on the substrate surface which blocked charge transfer path. With regard to NTETD concentration, the inhibiting influence is in the order: 300 mg/L > 200 mg/L > 100 mg/L > 400 mg/L > 50 mg/L.

Information on the corrosion resistance of metal sample in aggressive environment can be derived from impedance plot in

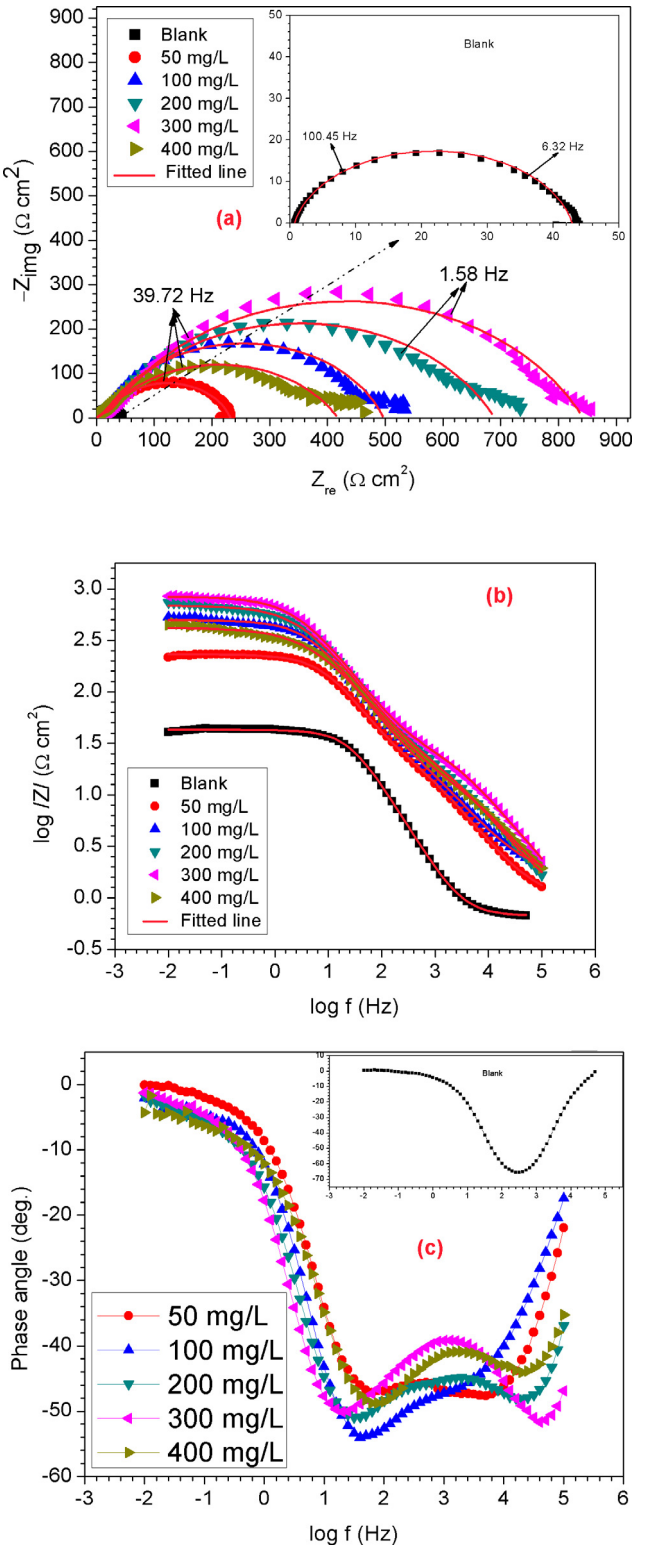

Fig. 4. Electrochemical impedance spectra for St37–2 steel in 15% HCl solution in the absence and presence of N-(2-(2-tridecyl-4,5-dihydro-1H-imidazol-1-yl)ethyl) tetradecanamide in (a) Nyquist and (b) Bode modulus representations at 25 °C.

the form of Bode modulus. In the low frequency region, increase in impedance modulus (Z_{mod}) infers better corrosion resistance [20,38]. Fig. 4(b) displays the Bode modulus representative graphs drawn for the metal substrate in studied acid solution without and with various dosages of NTETD at 25 °C. Clearly, there is a notice-

able Z_{mod} displacement in the inhibited acid solutions relative to that of the uninhibited solution. This shows that NTETD was effective in retarding the dissolution of the steel sample in the studied corrosive environment. The highest inhibiting effect is noted for NTETD concentration of 300 mg/L.

Fig. 4(c) presents the Phase angle versus frequency plots for the studied systems. In the Phase angle graph for the blank system, a single peak is observed whereas double peaks are noted in the graphs of the inhibited systems. These results indicate one-time and two-time constants in the uninhibited and inhibited systems, respectively. Accordingly, the unprotected system was described with a single-time constant model given in Fig. 5(a) while the protected systems were described using the two-time constant model shown in Fig. 5(b). The model in Fig. 5(a) consists of R_s, R_{ct} and *CPE* elements representing solution resistance, charge transfer resistance and constant phase element, respectively. The model in Fig. 5(b) has film resistance (R_f) as additional element. The impedance constant phase element (Z_{CPE}) can be expressed as [38]:

$$Z_{CPE} = \frac{1}{Y_0(jw)^n} \tag{4}$$

where Y_0 = quantity of *CPE*, j = imaginary unit ($j^2 = -1$), n = phase shift parameter ($n = 2\alpha/(\pi)$), w = angular frequency. The *CPE* components Y_0 and n were used in the calculation of the double layer capacitance (C_{dl}) of adsorbed film following Eq. (8) [40]:

$$C_{dl} = \left(Y_0 R_{ct}^{n-1}\right)^{1/n} \tag{5}$$

All the derived electrochemical parameters for the studied systems are listed in Table 1. The value of retardation efficiency (η_{EIS}) was computed using Eq. (6).

$$\eta_{EIS} = \left(1 - \frac{R^0}{R}\right) \times 100 \tag{6}$$

where R^0 and R are the charge transfer resistances in the absence and presence of NTETD respectively. It is clear from the results in Table 1 that the values of R (summation of resistances) and η_{EIS} increase while C_{dl} value decrease as the inhibitor dosage was increased from 50 mg/L to 300 mg/L. The maximum R and η_{EIS} obtained are 842.44 Ω cm^2 and 94.99% respectively while the least C_{dl} value is 4.77 mF cm^{-2} achieved by the 300 mg/L concentration. The observed increase in the R and η_{EIS} values and decrease in C_{dl} value with increasing inhibitor concentration is due to the gradual adsorption and replacement of adsorbed water molecules on the substrate surface which lowered the local dielectric constant and increase the thickness of electrical double layer [41]. Furthermore, the results in Table 1 reveal that beyond 300 mg/L, the resistance as well as the inhibition efficiency of NTETD decline. The concentration, 300 mg/L is therefore taken as the optimum concentration. At this concentration, maximum area on the steel electrode surface was covered by inhibitor molecules [42] but beyond it, the solution became saturated such that un-adsorbed and adsorbed molecules interacted [42]. Such interaction would give rise to desorption of adsorbed species [42,43] and desorption affects inhibition efficiency negatively.

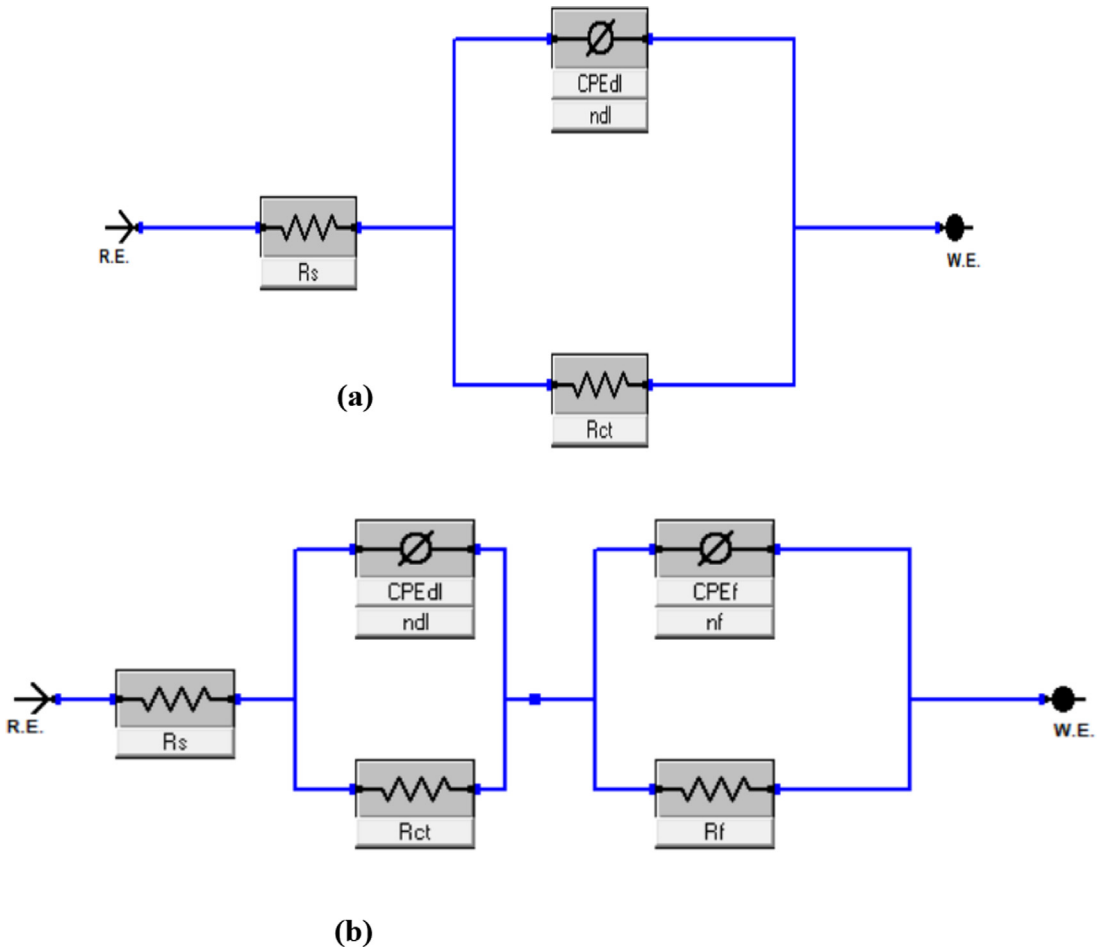

Fig. 5. Equivalent circuit diagrams used to fit impedance data in the (a) blank and (b) presence of N-(2-(2-tridecyl-4,5-dihydro-1H-imidazol-1-yl)ethyl)tetradecanamide.

Table 1
Electrochemical impedance parameters for St37 steel in 15% HCl solution in the absence and presence of different concentrations of N-(2-(2-tridecyl-4,5-dihydro-1H-imidazol-1-yl)ethyl)tetradecanamide at 25 °C.

Conc. (mg/L)	R_s (Ω cm^2)	CPE_{dl}		R_{ct} (Ω cm^2)	CPE_f		R_f (Ω cm^2)	R (Ω cm^2)	C_{dl} (mF cm^{-2})	$x^2 \times 10^{-3}$	η_{EIS}
		Y_{01} (mΩ^{-1} s^2 cm^{-2})	n_{dl}		Y_{02} (mΩ^{-1} s^2 cm^{-2})	n_f					
0	0.67 ± 0.05	0.27	0.88	42.18 ± 0.22	–	–	–	42.18	131.33	0.49	–
50	0.91 ± 0.04	0.68	0.80	214.80 ± 3.00	0.22	0.18	16.22 ± 0.01	231.02	93.59	0.22	81.74
100	1.59 ± 0.06	0.64	0.77	482.00 ± 4.23	0.15	0.32	13.71 ± 0.01	495.71	59.44	1.06	91.49
200	0.67 ± 0.07	0.17	0.72	673.60 ± 3.03	0.15	0.66	15.19 ± 0.01	688.79	6.63	1.27	93.88
300	0.46 ± 0.11	0.10	0.75	805.40 ± 3.17	0.05	0.68	37.04 ± 0.03	842.44	4.77	1.36	94.99
400	0.93 ± 0.08	0.23	0.72	409.50 ± 3.97	0.07	0.67	7.75 ± 0.08	417.25	31.52	2.22	89.89

3.2.3. PDP and LPR studies

To further gain insight into the influence of NTETD on the anodic and the cathodic corrosion reactions of St37-2 steel in the studied corrodent, potentiodynamic polarization measurements were performed and the results in graphical form is shown in Fig. 6. In the figure, the corrosion inhibition effect of NTETD is reflected on the displacement of the anodic and cathodic curves to lower current densities relative to the blank. The displacement is rather more pronounced on the cathodic branch than anodic and thus agree with the OCP results that NTETD functioned in the studied system as a mixed type inhibitor but under cathodic control. Additionally, both the anodic and cathodic branches show Tafel-like regions; meaning the corrosion kinetics were activation controlled [44,45]. Therefore, the two branches were extrapolated to obtain the polarization parameters namely, corrosion current density (i_{corr}), corrosion potential (E_{corr}), anodic Tafel slope (β_a), and cathodic Tafel slope (β_c). Values for these parameters are listed in Table 2. The inhibition efficiency (η_{PDP}) of NTETD from this technique was computed using Eq. (7) while the values of corrosion rate (v, mm/yr) also given in Table 2 was estimated using the following Eq. (8) [46]:

$$\eta_{PDP} = \left(1 - \frac{i_{corr}}{i^0_{corr}}\right) \times 100 \tag{7}$$

$$v = 3.27 \times i_{corr} \times \frac{e}{\rho} \tag{8}$$

where i^0_{corr} and i_{corr} are corrosion current densities, respectively in the absence and presence of NTETD, 3.27 is a proportionality constant, e and ρ the equivalent weight and density of steel, respectively. i_{corr} is expressed in mA cm^{-2}. It is obvious from Table 2 that the presence of NTETD in 15% HCl solution significantly drained the corrosion current and as effect decreased the corrosion rate of the metal electrode. The presence of 50 mg/L NTETD reduced the i_{corr} and v from 422.00 μA cm^{-2} and 4.97 mm/yr respectively to 62.00 μA cm^{-2} and 0.73 mm/yr and this correspond to inhibition efficiency of 85.31%. At optimum concentration (300 mg/L), the i_{corr} and v attained the lowest values of 27.90 μA cm^{-2} and 0.33 mm/yr respectively and the metal surface was protected by 93.38%. The change between β_c values of inhibited systems and that of the uninhibited is more significant than that of β_a. For instance, the difference between β_c value of 50 mg/L NTETD inhibited system and that of the blank is 44.9 mV dec^{-1} whereas the difference between β_a value of the same concentration and β_a value of blank is 23.6 mV dec^{-1}. This again points to the principal cathodic effect by NTETD.

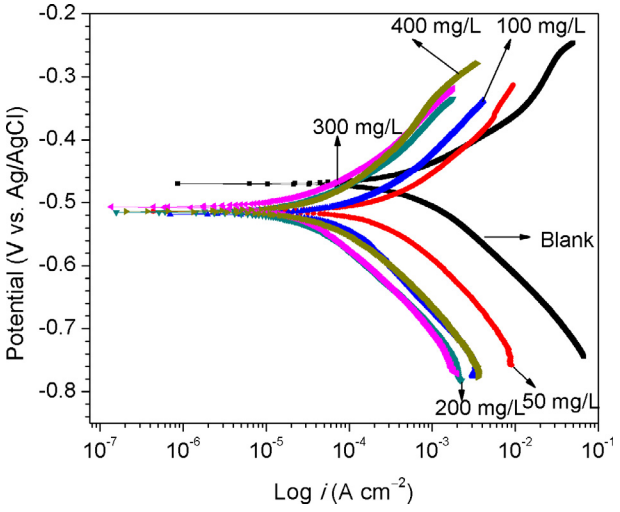

Fig. 6. Potentiodynamic polarization plots for St37-2 steel in 15% HCl solution without and with different concentrations of N-(2-(2-tridecyl-4,5-dihydro-1H-imidazol-1-yl)ethyl)tetradecanamide at 25 °C.

The corrosion inhibition of St37-2 steel in 15% HCl medium by NTETD was also studied using linear polarization (LPR) approach. The obtained polarization resistance (R_p) and the calculated inhibition efficiency (Eq. (9)) are also presented in Table 2. The R_p increased in the presence of inhibitor up to 843.10 Ω cm^2 at 300 mg/L NTETD concentration. The protection efficiency of the optimum concentration from this technique is 95.60% which is in excellent agreement which those from EIS (Table 1) and PDP (Table 2) techniques.

$$\eta_{LPR} = \left(1 - \frac{R^0_p}{R_p}\right) \times 100 \tag{9}$$

where R^0_p and R_p are the polarization resistance respectively in the absence and presence of NTETD.

3.2.4. Weight loss studies

The weight loss technique, up till now remains a reliable and simplest approach for determining the rate of metal corrosion and the efficacy of a corrosion inhibitor in a corrosive environment. It is a direct corrosion measuring technique and provides information on the average corrosion rate as such requires long exposure times [47]. Despite the long experimental duration required, procedure can be replicated easily and this reduces the tendency of introducing systematic errors. This technique was also adopted in the study of the low carbon steel dissolution in the studied corrosive environment unprotected and protected with diverse dosages of NTETD at 25 °C. The obtained results are given in Table 3. The weight loss and corrosion rate of St37-2 steel in 15% HCl containing NTETD was minimal compared to the unprotected acid solution. The presence of 50 mg/L NTETD in the acid solution was sufficient to reduce the corrosion rate of the metal sample from 20.78 mm/yr to 1.07 mm/yr. The corrosion rate in the presence of other concentrations of NTETD (100–400 mg/L) was less than unity. Interestingly, all the concentrations of NTETD could offer corrosion protection of above 93% to the metal surface. This

Table 2
Corrosion parameters for St37 steel in 15% HCl solutions in the absence and presence of different concentrations of N-(2-(2-tridecyl-4,5-dihydro-1H-imidazol-1-yl)ethyl) tetradecanamide at 25 °C from potentiodynamic polarization (PDP) and linear polarization (LPR) methods.

Conc. (mg/L)	PDP						LPR	
	- E_{corr} (mV vs. Ag/AgCl)	i_{corr} (μA cm^{-2})	β_a (mV dec^{-1})	β_c (mV dec^{-1})	v (mm/yr)	η_{PDP} (%)	R_p (Ω cm^2)	η_{LPR} (%)
0	470.00	422.00	74.10	84.10	4.97	–	39.09	–
50	514.00	62.00	97.70	129.00	0.73	85.31	229.10	82.94
100	518.00	51.20	97.50	253.30	0.60	87.87	484.70	91.94
200	515.00	42.30	137.70	223.00	0.49	89.98	801.80	95.12
300	507.00	27.90	86.70	122.60	0.33	93.38	843.10	95.60
400	514.00	43.60	97.80	86.60	0.52	89.67	467.80	91.64

Table 3
Calculated values of weight loss (g), corrosion rate (mm y^{-1}), surface coverage (θ), and inhibition efficiency (η) for St37 steel in 15% HCl solution from weight loss measurements at 25 °C.

Concentration (mg/L)	Weight loss (g) × 10^{-3}	v (mm y^{-1})	θ	η(%)
0	100.5 ± 0.03	20.78	–	–
50	5.2 ± 0.02	1.07	0.95	94.83
100	4.0 ± 0.02	0.83	0.96	96.02
200	3.8 ± 0.04	0.79	0.96	96.22
300	3.5 ± 0.03	0.72	0.97	96.51
400	3.7 ± 0.03	0.76	0.96	96.32

is a clear demonstration of the high inhibitive strength of NTETD which could be explained on the basis of the strong interaction between NTETD molecules and the steel surface. There are three potential interaction centers in NTETD, which are, the N, O, and imidazoline ring (Fig. 1(d)). Through these centers, the inhibitor can adsorb on the substrate surface and cover corrosion reaction sites and as effect, decrease the corrosion rate. The total surface area covered by adsorbed inhibitor molecules plays important role on the level of protection offered. The larger the surface area covered, the higher the protection rendered. In the studied systems, the NTETD molecules nearly covered the entire St37-2 sample surface as suggested by the near unity values of θ in Table 3. Regarding the variation of inhibition efficiency with inhibitor concentration, the trend noted in the electrochemical results (Tables 1 and 2) is also observed, that is, inhibition efficiency varies directly with inhibitor dosage up to 300 mg/L but decreases afterward. The highest inhibition efficiency as offered by the optimum concentration is 96.52%. It should be mentioned that the weight loss results are in conformity with the electrochemical results (Tables 1 and 2).

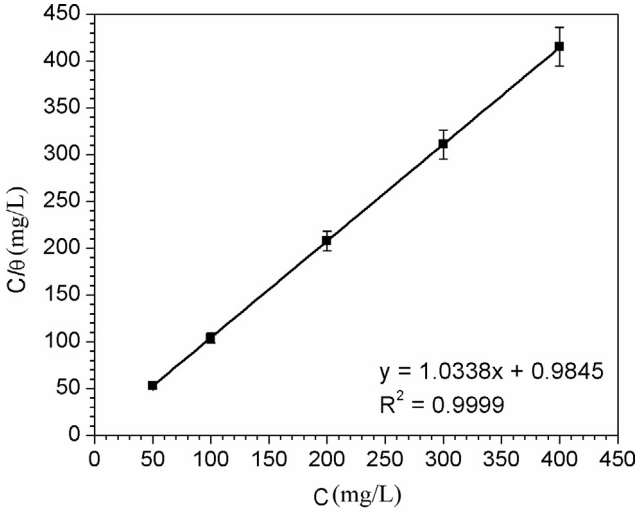

Fig. 7. Langmuir isotherm plot for N-(2-(2-tridecyl-4,5-dihydro-1H-imidazol-1-yl) ethyl)tetradecanamide adsorption on St37 steel in 15% HCl.

3.3. Adsorption studies

Information from adsorption isotherm can be used to estimate the strength of interaction between adsorbed species and substrate surface as well as the spontaneity of adsorption process. To explain the adsorption of NTETD molecules on St37-2 steel surface in studied environment, the values of θ given in Table 3 were fitted into Langmuir isotherm model which assumes the general form:

$$\frac{C_{inh}}{\theta} = \frac{1}{K_{ads}} + C_{inh} \quad (10)$$

where K_{ads} is adsorption-desorption equilibrium constant and define the strength of the bond between adsorbent and adsorbate [48]. C_{inh} is the dosage of NTETD in mg/L. A plot of C_{inh}/θ as a function of C_{inh} resulted in a linear graph given in Fig. 7 with regression coefficient (R^2) of 0.9999. This shows that the adsorption of NTETD molecules on St37-2 steel surface obeyed the Langmuir adsorption isotherm model. Additional proof is the value of the slope (1.03386) which can be approximated to unity required for an ideal Langmuir adsorption isotherm model. The value of K_{ads} was computed from the intercept of the graph and is 1.015 × 10^3. The large value of K_{ads} indicates strong adsorption bond between NTETD molecules and St37-2 steel surface. Normally, such strong interaction is common with chemisorption mechanism. In the chemical adsorption of *N*-phenyl-1-(4-((11-(pyridin-1-ium-1yl) undecanoyl) oxy)phenyl) methanimine oxide bromide on St37 surface in HCl medium, K_{ads} value of 58.82 × 10^3 was reported [33]. Zhang et al. [17] reported K_{ads} value of 291,247 for the chemical adsorption of imidazoline-based inhibitor on low alloy steel in CO_2-saturated NaCl medium. Similarly, Solomon et al. [49] reported K_{ads} value in the range of 43–103 × 10^3 for the chemisorption of carboxymethyl cellulose/silver nanoparticles composite on St37 steel surface in sulphuric acid solution. The electron pair in the heteroatoms present in NTETD molecules as well as the pi electron in the imidazoline ring (Fig. 1 (d)) can be utilized for p-d type of bonding with the steel surface. The electron pair can be donated to the 3d orbital of iron and covalent bond is formed. The K_{ads} value was deployed in the computation of the standard free energy of adsorption (ΔG^0_{ads}) as follows [32]:

$$\Delta G^0_{ads} = -RT\ln\left(1 \times 10^6 K_{ads}\right) \quad (11)$$

where 1×10^6 is the concentration of water molecules (same as concentration of inhibitor) in mg/L, R and T are the molar gas constant (8.3144598 J/K) and absolute temperature respectively. The calculated ΔG^0_{ads} value is -27.10 kJ mol^{-1} and this infers spontaneous adsorption of NTETD molecules onto St37-2 steel surface [33].

3.4. Surface morphological studies

3.4.1. SEM and EDAX studies

In Fig. 8 is shown the SEM images and EDAX spectra obtained for low carbon steel specimen exposed to 15% HCl solution in the absence and presence of NTETD for 24 h at room temperature. Obviously, the specimen surface was damaged in the acid solution. The corrosive attack resulted in rough surface morphology as seen in Fig. 8(a). Some cracks can as well be spotted on the surface. The corresponding EDAX spectrum in Fig. 8(b) reveals additional elements i.e Cl and O to the steel basic component elements (Fe, C, Mn) on the surface. This suggests that the corrosion products on the surface are mixture of chlorides and oxides. Compared with Fig. 8(a), the surface in Fig. 8(c) is more uniform and free of cracks. The adsorption of NTETD molecules on the surface may have protected the surface from corrosive attacks. In the inserted table in Fig. 8(d), the wt.% of Fe and Cl is lesser while that of C is higher than those in the inserted table in Fig. 8(b). The increase of wt.% of C from 6.1% to 10.3% may be due to adsorption of NTETD. The decrease of wt.% of Fe and Cl from 83.4% and 6.0% to 80.3% and 2.3%, respectively in the surface exposed to inhibited system may be due to the coverage of the surface by the adsorbed inhibitor layer. However, the N component element of NTETD was not

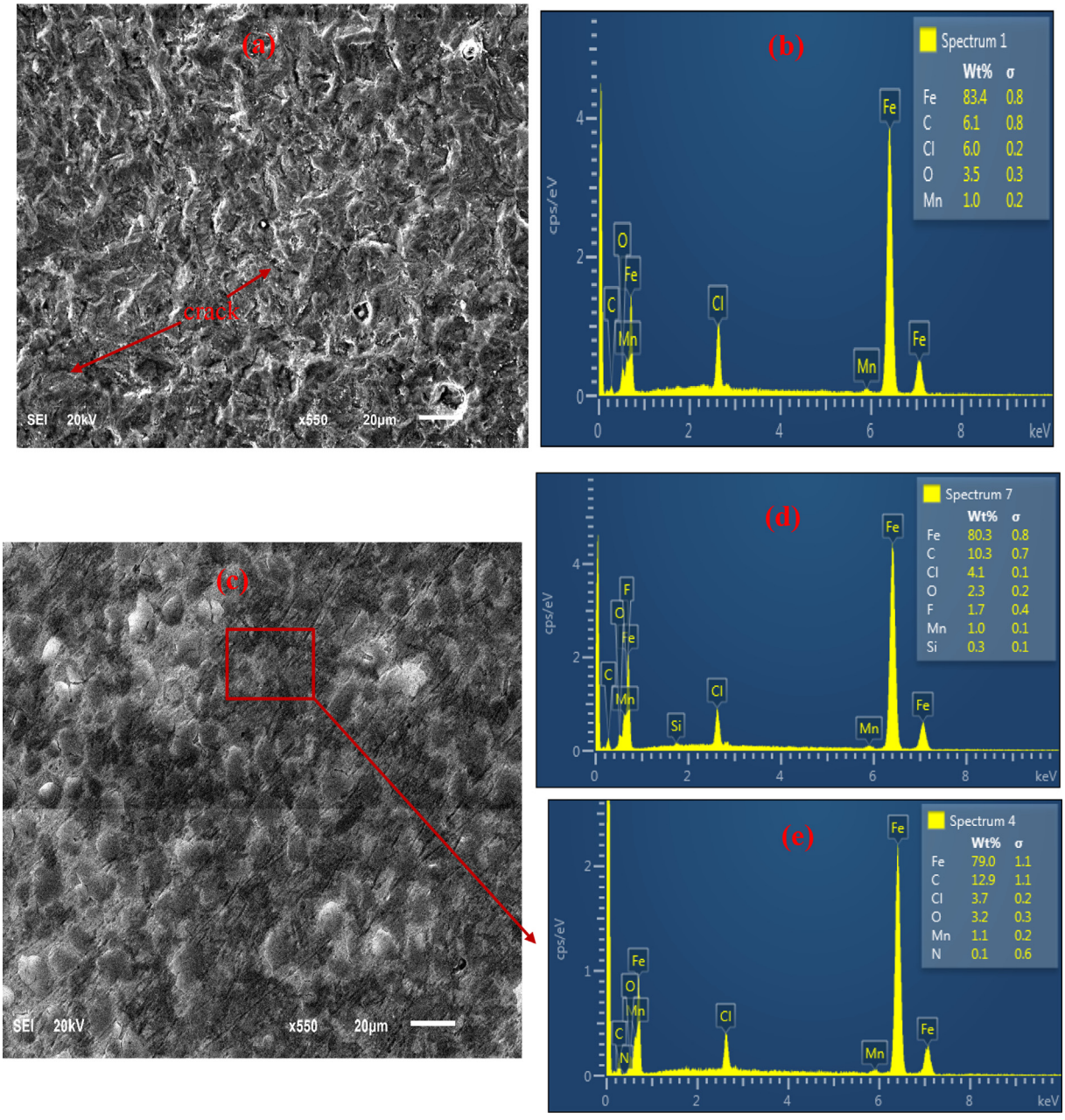

Fig. 8. SEM pictures and EDAX spectra for St37–2 steel sample after immersion in 15% HCl solution (a and b) without N-(2-(2-tridecyl-4,5-dihydro-1H-imidazol-1-yl)ethyl) tetradecanamide, and (c–e) containing 300 mg/L N-(2-(2-tridecyl-4,5-dihydro-1H-imidazol-1-yl)ethyl)tetradecanamide for 24 h at 25 °C.

detected when the entire surface was scanned but detected when a specific deposit film spot was scanned (Fig. 8(e)). The N heteroatoms may have been used for the adsorption process.

3.4.2. AFM studies

Information regarding the roughness property of a surface can be deduced from AFM surface screening. In Fig. 9 is presented the 2-dimensional and 3-dimensional AFM pictures taken from the steel sample after exposure to 15% HCl solution devoid of and containing NTETD for 24 h at 25 °C. The ISO (International Organization of Standardization) has listed certain parameters for the characterization of a surface and they include R_p (maximum band height), R_v (maximum valley depth), R_z (mean band to valley height), R_c (mean band to valley height with no limit to the amount of peaks and valleys), R_t (largest band to valley height), R_a (mean value of profile deviation from mean line), R_q (root-mean-square deviation from a profile), RS_m (mean spacing of profile elements), and Rdq (root mean square slope of examined profile) [24,50,51]. The values of these parameters for the studied surfaces are given in the tables inserted in Fig. 9. The studied inhibitor was effective in protecting the steel sample surface in the corrosive environment. As could be seen in the figure, the 2D and 3D images in Fig. 9(b) look smoother compared to the 2D and 3D pictures in Fig. 9(a). There is reduction in the values of all the roughness parameters in Fig. 9(b) inserted table relative to the values in the table inserted in Fig. 9(a). The R_a and R_q values are remarkably reduced, i.e from 0.183 μm and 0.216 μm in the unprotected surface to 0.055 μm and 0.067 μm in the protected surface. All these portray NTETD as being capable of steel corrosion retardation in strong acid medium.

3.4.3. FTIR studies

The claim of adsorption of NTETD molecules on St37-2 steel specimen surface was also verified by FTIR studies. The FTIR spectrum of adsorbed films extracted from the surface of steel sample immersed in 15% HCl solution containing 300 mg/L NTETD for 24 h at ambient temperature is given in Fig. 10. As could be seen, the spectrum in Fig. 10 is similar to the FTIR spectrum of the pure NTETD (Fig. 2(b)) and thus confirms the adsorption of NTETD molecules on the surface. However, there exist some differences in the FTIR spectrum of the pure NTETD (Fig. 2(b)) and that of the extracted film (Fig. 10). For instance, the prominent C=O and N—H stretching bands at 1637 cm^{-1} and 3290 cm^{-1} in Fig. 2(b) are less intense in the extracted firm FTIR spectrum (Fig. 10). Again, the imidazoline ring N—H stretching peak at 1569 cm^{-1} in Fig. 2(b) is absent in Fig. 10. This observation indicates that the heteroatoms (N and O) were involve in the interaction between NTETD molecules and the steel surface. Similar submission can be found in the corrosion literature [49,52].

3.4.4. XPS studies

The high resolution and XPS survey spectra obtained for the steel specimen surface immersed in studied corrodent for a day at ordinary temperature are displayed in Fig. 11. In the surface,

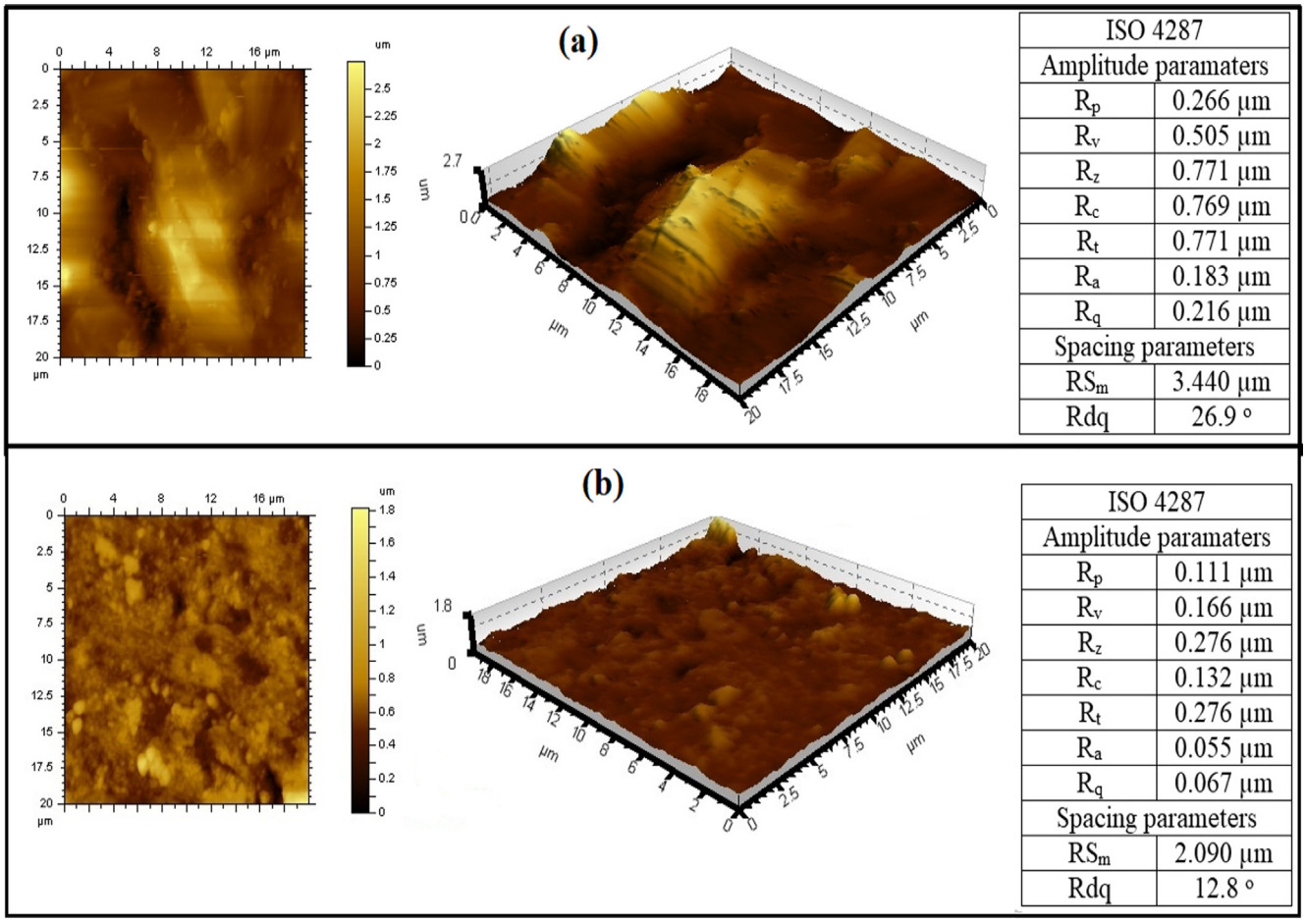

ISO 4287	
Amplitude paramaters	
R_p	0.266 μm
R_v	0.505 μm
R_z	0.771 μm
R_c	0.769 μm
R_t	0.771 μm
R_a	0.183 μm
R_q	0.216 μm
Spacing parameters	
RS_m	3.440 μm
Rdq	26.9 °

ISO 4287	
Amplitude paramaters	
R_p	0.111 μm
R_v	0.166 μm
R_z	0.276 μm
R_c	0.132 μm
R_t	0.276 μm
R_a	0.055 μm
R_q	0.067 μm
Spacing parameters	
RS_m	2.090 μm
Rdq	12.8 °

Fig. 9. AFM photographs in 2D and 3D formats for St37–2 steel specimen after immersion in 15% HCl solution (a) free from and (b) containing 300 ppm N-(2-(2-tridecyl-4,5-dihydro-1H-imidazol-1-yl)ethyl)tetradecanamide for 24 h at 25 °C. Inserted table shows the roughness parameters as defined by the ISO 4287 standard.

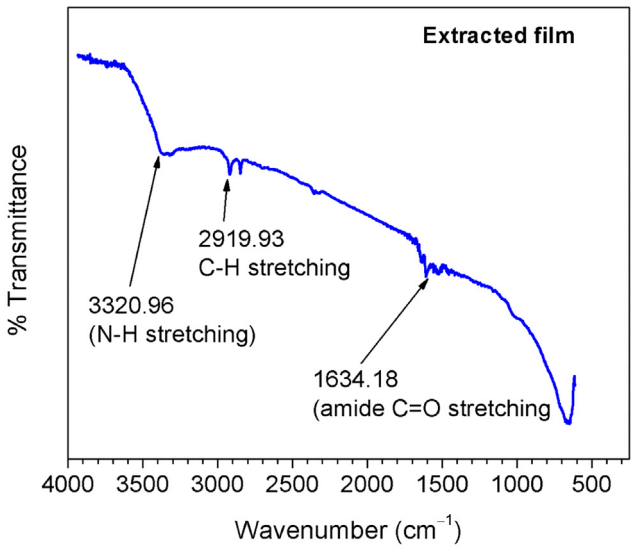

Fig. 10. FTIR spectrum of films extracted from St37–2 steel specimen surface after immersion in 15% HCl solution containing 300 mg/L N-(2-(2-tridecyl-4,5-dihydro-1H-imidazol-1-yl)ethyl)tetradecanamide for 24 h at 25 °C.

Cl, C, O, Fe were detected. This is in good agreement with the EDAX results. The Fe 2p high resolution spectrum exhibits peak at 710.48 eV, 716.28 eV, 723.98 eV, and 730.38 eV. The peaks at 710.48 eV and 723.98 eV are assigned to Fe species in ferric compounds like $FeCl_3$, FeO, FeOOH, and Fe_2O_3 [53–55]. Bands at 716.28 eV and 730.38 eV are associated with satellite of Fe^{3+} [55,56] and ferrhydrates [55,57] respectively. The peak at 198.88 eV and 200.88 eV in the Cl 2p spectrum are consistent with the Cl $2p_{3/2}$ and Cl $2p_{1/2}$ and infer Fe—Cl in compounds like $FeCl_2$ and $FeCl_3$ [55,57]. Three energy bands are seen in the C 1s at 285.48 eV, 289.08 eV, and 293.58 eV. The energy band at 285.48 eV and 289.48 eV are linked to C—O [55,56] and O—C=O [55,56] bonds. The implication of this results is that, the steel specimen corroded in HCl solution and mixture of oxides, chlorides, hydroxides, and carbonates may have constituted the corrosion products.

Fig. 12 shows the XPS survey and high resolution XPS spectra of the adsorbed films formed on studied specimen surface immersed in 15% HCl solution fortified with 300 mg/L NTETD for 24 h at 25 °C. All the elements detected in the surface exposed to the free acid solution were equally detected in the surface exposed to NTETD inhibited system. Additionally, nitrogen was detected which further proves the adsorption of NTETD molecules on the surface. In the N 1s spectrum, the energy bands at 400.78 eV is the most prominent with atomic weight of 86.97% and is assigned to the protonated amine group [58] in the synthesized compound. However, two other peaks are observed at 403.78 eV and 406.18 eV. The origin of these peaks is not well understood. According to Moschona et al. [59], bands at these binding energies are connected with nitrite or nitrate formation, and arise from the

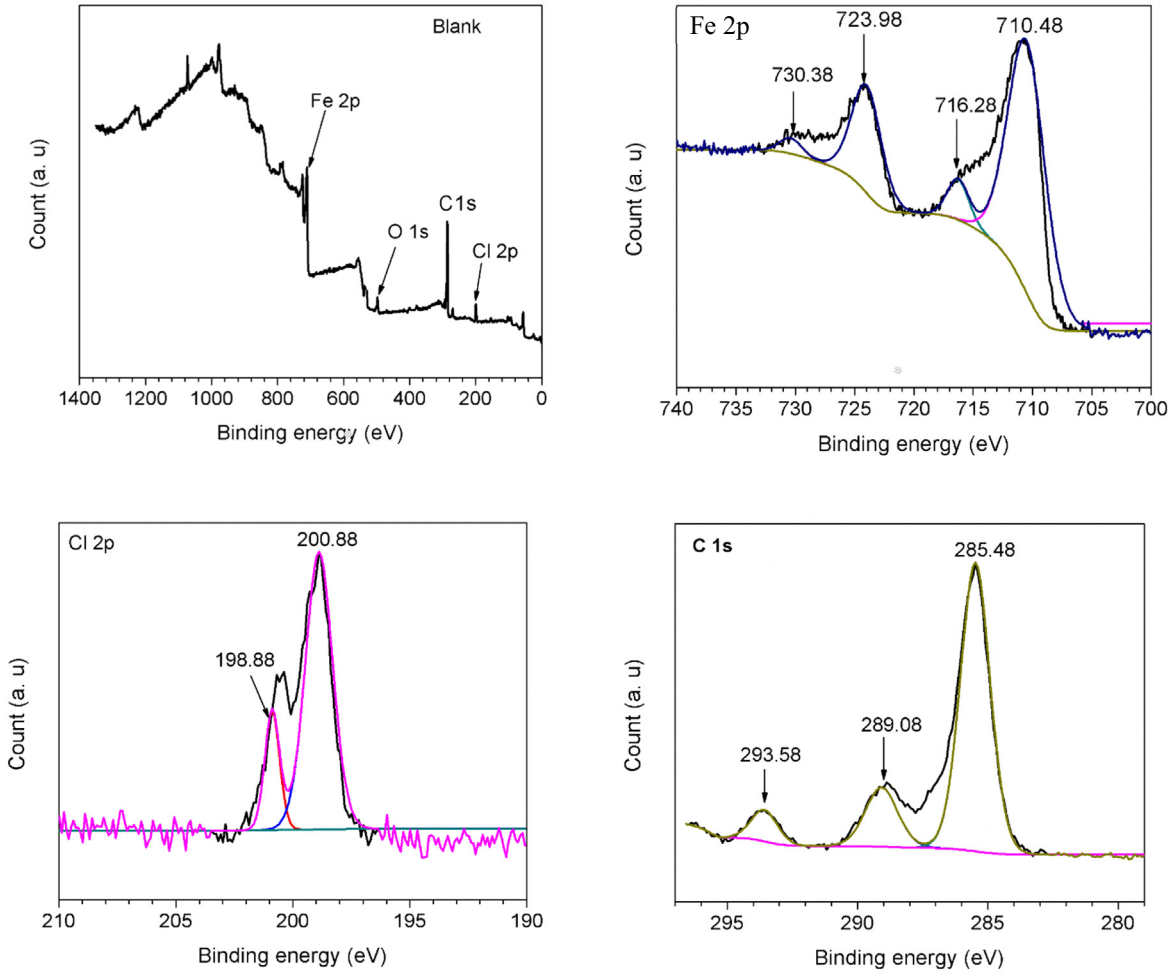

Fig. 11. XPS survey and high resolution XPS spectra of the corrosion products formed on St37–2 steel specimen surface immersed in 15% HCl solution for 24 h at 25 °C.

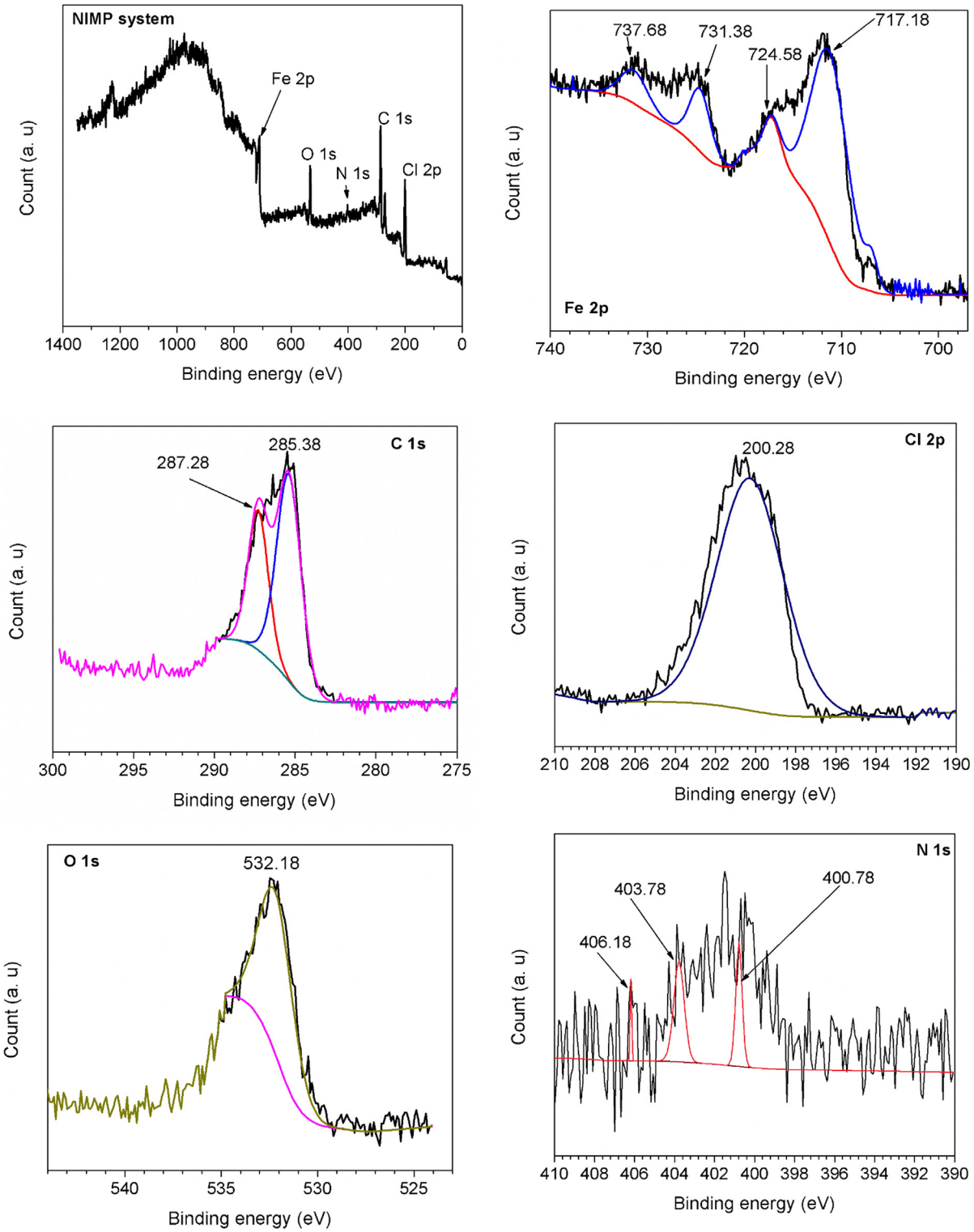

Fig. 12. XPS survey and high resolution XPS spectra of the adsorbed films formed on St37–2 steel specimen surface immersed in 15% HCl solution containing 300 mg/L N-(2-(2-tridecyl-4,5-dihydro-1H-imidazol-1-yl)ethyl)tetradecanamide for 24 h at 25 °C.

electronegative oxygen reducing the charge density on the nitrogen. The energy band associated with the C═O bond of the inhibitor is found at 532.18 eV [60] in the O 1s spectrum. The Cl $2p_{3/2}$ energy band noted in Fig. 11 is absent in the Cl 2p spectrum in Fig. 12 and might mean reduction in the chloride content on the specimen surface.

3.5. Corrosion inhibition mechanism by NTETD

It is generally accepted that corrosion inhibition by organic inhibitor involves the replacement of adsorbed H_2O molecules by inhibitor species [61–63]. It has been reported that steel surface in strong acid like the one herein considered acquires net positive

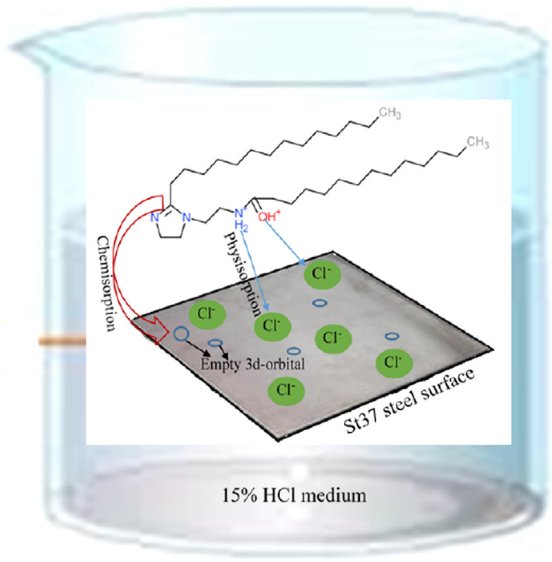

Fig. 13. Schematic illustration of the corrosion inhibition of St37-2 steel by N2245IMD in 15% HCl solution.

charge [64]. In HCl medium, chloride ions are specifically adsorbed on charged steel surface. Steel surface hydrated with chloride ions would have excess negative charges. In HCl solution, the nitrogen and perhaps the oxygen heteroatoms in the pendant group of NTETD (Fig. 1(d)) are protonated as revealed by the XPS result. Meanwhile, there are three possible adsorption centers in NTETD, i.e N, O, and the imidazoline ring. Cationic form of NTETD could be electrostatically attracted to charged steel surface and on the surface, electron pairs could be donated from the imidazoline ring to the low energy 3d-orbital of Fe (Fig. 13). The calculated value of K_{ads} suggested that the mechanism of adsorption of NTETD molecules on the steel surface was chemisorption. Also, NTETD has a long hydrophobic myristic acid pendant group (Fig. 1(d)). This group can as well cover the metal surface and limit the ingression of corrosion ions. The high inhibition efficiency exhibited by NTETD (i.e > 90%) is therefore due to the barrier effect by its pendant group, physical, and chemical interactions of its heteroatoms with steel surface.

4. Conclusion

Imidazolines are sensitive to hydrolysis reverting to products with little or no anticorrosion property [11,12]. Nevertheless, introduction of suitable substituent(s) and on an appropriate site (s) can offset the effect [13,14]. The description given for an effective imidazoline-based corrosion inhibitor is that, the chain length of the pendant group should be greater than twelve and attached on the ring nitrogen atom or on a relatively small organic radical attached to one of the nitrogen atoms of the ring [13,14]. Based on this description, we have successfully synthesized an imidazoline compound from myristic acid and diethyleneamine. The synthesized compound, N-(2-(2-tridecyl-4,5-dihydro-1H-imidazol-1-yl)ethyl)tetradecanamide (NTETD) has been tested as a corrosion inhibitor for low carbon steel in 15% HCl solution. NTETD is effective and the optimum concentration (300 mg/L) reduced the corrosion rate of low carbon steel in the studied corrosive environment from 20.78 mm/yr to 0.72 mm/yr corresponding to inhibition efficiency of 96.51%. This is comparable with the inhibition efficiency of 97.92% reported for N-(2-(2-pentadecyl-4,5-dihydro-1H-imidazol-1-yl)ethyl)palmitamide in the same corrosive medium [22]. The corrosion inhibition effect was by virtue of adsorption onto the substrate's surface as confirmed by the XPS results and can be explained using the Langmuir adsorption isotherm model. Furthermore, NTETD acted as a mixed type corrosion inhibitor but with principal effect on cathodic corrosion half reactions. The mechanism of corrosion inhibition proposed is chemisorption whereby electron pairs are denoted by NTETD to the 3d orbital of Fe [17].

Declaration of Competing Interest

The authors declare no conflict of interest.

References

[1] L. Gandossi, An overview of hydraulic fracturing and other formation stimulation technologies for shale gas production, Europ. Comm. Joint Res. Centre Tech. Rep. (2013), https://doi.org/10.2790/99937.
[2] G. L. McClung IV. Acidizing materials and methods and fluids for earth formation protection. US 20130333892 A1, U.S. Patent 2013, Application No. 13/815,494.
[3] L. Kalfayan. Production enhancement with acid stimulation. Pennwell Books 2008, Tusla, Okla.
[4] M.U. Shafiq, M.T. Shuker, A. Kyaw, Performance comparison of new combinations of acids with mud acid in sandstone acidizing, RJASET 7 (2) (2014) 323–328.
[5] S.N. Rana Corrosion inhibition study of carbon steel A515 in sour water at 75 oC. M. Sc. thesis, University of Technology, Ministry of Higher Education & Scientific Research, Republic of Iraq, DOI: 10.13140/RG.2.1.4782.8008.
[6] J.M. Zhao, J. Li, Corrosion inhibition performance of carbon steel in brine solution containing H_2S and CO_2 by novel gemini surfactants, Acta Phys.-Chim. Sini. 28 (2012) 623–629.
[7] A.J. Szyprowski, Relationship between chemical structure of imidazoline inhibitors and their effectiveness against hydrogen sulphide corrosion of steels, Br. Corros. J. 35 (2000) 155–160.
[8] E. A. Reyes, A. L. Lablanc, A. M. Beuterbaugh. Corrosion inhibition of HCl treatment fluids with environmentally compatible solvent. Patent No.: US 20180127882 A1, May 2018.
[9] H. Liu, D.M. Du, Recent advances in the synthesis of 2-imidazolines and their applications in homogeneous catalysis, Adv. Synth. Catal. 351 (2009) 489–519.
[10] C. Dardonville, I. Rozas, Imidazoline binding sites and their ligands: an overview of the different chemical structures, Med. Res. Rev. 24 (2004) 639–661.
[11] M.M. Wafts, Imidazoline hydrolysis in alkaline and acidic media-a review, J. Am. Oil. Chem. Soc. 67 (12) (1990) 993.
[12] G. R. Meyer. Corrosion inhibition compositions. US Patent US 6303079 B1, 2001.
[13] S. Ramachandran, B. Tsai, M. Blanco, H. Chen, Y. Tang, W.A. Goddard, Self-assembled monolayer mechanism for corrosion inhibition of iron by imidazolines, Langmuir 12 (1996) 6419–6428.
[14] C. M. Blair, Jr., W. Groves, W. F. Gross. Processes for preventing corrosion and corrosion inhibitors. US Patent No.: 2,466,517, April, 1949.
[15] H. Zhang, K. Gao, L. Yan, X. Pang, Inhibition of the corrosion of X70 and Q235 steel in CO2-saturated brine by imidazoline-based inhibitor, J. Electroanal. Chem. 791 (2017) 83–94.
[16] Y.Z. Li, N. Xu, X.P. Guo, G.A. Zhang, Inhibition effect of imidazoline inhibitor on the crevice corrosion of N80 carbon steel in the CO_2-saturated NaCl solution containing acetic acid, Corros. Sci. 126 (2017) 127–141.
[17] H. Zhang, X. Pang, M. Zhou, C. Liu, L. Wei, K. Gao, The behavior of pre-corrosion effect on the performance of imidazoline-based inhibitor in 3 wt.% NaCl solution saturated with CO_2, Appl. Surf. Sci. 356 (2015) 63–72.
[18] H. Zhang, X. Pang, K. Gao, Localized CO_2 corrosion of carbon steel with different microstructures in brine solutions with an imidazoline-based inhibitor, Appl. Surf. Sci. 442 (2018) 446–460.
[19] L. Zhang, Y. He, Y. Zhou, R. Yang, Q. Yang, D. Qing, Q. Niu, A novel imidazoline derivative as corrosion inhibitor for P110 carbon steel in hydrochloric acid environment, Petroleum 1 (2015) 237–243.
[20] X. He, Y. Jiang, C. Li, W. Wang, B. Hou, L. Wu, Inhibition properties and adsorption behavior of imidazole and 2-phenyl-2-imidazoline on AA5052 in 1.0 M HCl solution, Corros. Sci. 83 (2014) 124–136.
[21] M. Yadav, D. Behera, U. Sharma, Nontoxic corrosion inhibitors for N80 steel in hydrochloric acid, Arab. J. Chem. 9 (2016) S1487–S1495.
[22] M.M. Solomon, S.A. Umoren, M.A. Quraishi, M.A. Jafar Mazumder, Corrosion inhibition of N80 steel in simulated acidizing environment by N-(2-(2-pentadecyl-4,5-dihydro-1H-imidazol-1-YL) ethyl) palmitamide, J. Mol. Liq. 273 (2019) 476–487.
[23] D. Bajpai, V.K. Tyagi, Microwave synthesis of cationic fatty imidazolines and their characterization, J. Surfact. Deterg. 11 (2008) 79–87.
[24] M.M. Solomon, S.A. Umoren, I.B. Obot, A.A. Sorour, H. Gerengi, Exploration of dextran for application as corrosion inhibitor for steel in strong acid environment: effect of molecular weight, modification, and temperature on efficiency, ACS Appl. Mater. Interfaces 10 (2018) 28112–28129.
[25] ASTM-G 01–03, ASTM Book of Standards, West Conshohocken: ASTM, 2003, vol. 3.02.

[26] ASTM-G 01–90, Standard practice for preparing, cleaning, and evaluation corrosion test specimens, ASTM Book of Standards (Reapproved 1999).
[27] ASTM G3-89, Conventions applicable to electrochemical measurements in corrosion testing, Annual Book of ASTM standard 30 (Reapproved 1994).
[28] ASTM G3-94, Making potentiostatic and potentiodynamic anodic polarization measurements, Annual Book of ASTM standard 48 (Reapproved 1994).
[29] G. Sıgırcık, T. Tüken, M. Erbil, Assessment of the inhibition efficiency of 3, 4-diaminobenzonitrile against the corrosion of steel, Corros. Sci. 102 (2016) 437–445.
[30] A.P. Srikanth, T.G. Sunitha, V. Raman, S. Nanjundan, N. Rajendran, Synthesis, characterization and corrosion protection properties of poly (n-(acryloyloxymethyl) benzotriazole-co-glycidyl methacrylate) coatings on mild steel, Mater. Chem. Phys. 103 (2007) 241–247.
[31] E.E. Oguzie, Y. Li, F.H. Wang, Corrosion inhibition and adsorption behavior of methionine on mild steel in sulphuric acid and synergistic effect of iodide ion, J. Colloid Interface Sci. 310 (2007) 90–98.
[32] M.M. Solomon, S.A. Umoren, In-situ preparation, characterization and anticorrosion property of polypropylene glycol/silver nanoparticles composite for mild steel corrosion in acid solution, J. Colloid Interface Sci. 462 (2016) 29–41.
[33] H. Gerengi, M.M. Solomon, S. Öztürk, A. Yıldırım, G. Gece, E. Kaya, Evaluation of the corrosion inhibiting efficacy of a newly synthesized nitrone against St37 steel corrosion in acidic medium: experimental and theoretical approaches, Mater. Sci. Eng., C 93 (2018) 539–553.
[34] M. Ramezanzadeh, G. Bahlakeh, Z. Sanaei, B. Ramezanzadeh, Corrosion inhibition of mild steel in 1 M HCl solution by ethanolic extract of eco-friendly *Mangifera indica (mango)* leaves: electrochemical, molecular dynamics, Monte Carlo and ab initio study, Appl. Surf. Sci. 463 (2019) 1058–1077.
[35] S.A. Haladu, S.A. Umoren, S.A. Ali, M.M. Solomon, A.I. Mohammed, Synthesis, characterization and electrochemical evaluation of anticorrosion property of a tetrapolymer for carbon steel in strong acid media, Chin. J. Chem. Eng. (2018), https://doi.org/10.1016/j.cjche.2018.07.015.
[36] J. Pan, D. Thierry, C. Leygraf, Electrochemical impedance spectroscopy study of the passive oxide film on titanium for implant application, Electrochim. Acta 41 (1996) 1143–1153.
[37] Z.B. Wang, H.X. Hu, Y.G. Zheng, W. Ke, Y.X. Qiao, Comparison of the corrosion behavior of pure titanium and its alloys in fluoride-containing sulfuric acid, Corros. Sci. 103 (2016) 50–65.
[38] M. Das, A. Biswas, B.K. Kundu, S.M. Mobin, G. Udayabhanu, S. Mukhopadhyay, Targeted synthesis of cadmium(II) Schiff base complexes towards corrosion inhibition on mild steel, RSC Adv. 7 (2017) 48569–48585.
[39] K. Zhang, W. Yang, B. Xu, Y. Liu, X. Yin, Y. Chen, Corrosion inhibition of mild steel by bromide-substituted imidazoline in hydrochloric acid, J. Taiwan Inst. Chem. Eng. 57 (2015) 167–174.
[40] N. El Hamdani, R. Fdil, M. Tourabi, C. Jama, F. Bentiss, Alkaloids extract of *Retama monosperma* (L.) Boiss. seeds used as novel eco-friendly inhibitor for carbon steel corrosion in 1M HCl solution: electrochemical and surface studies, Appl. Surf. Sci. 357 (2015) 1294–1305.
[41] A.S. Fouda, M.A. Ismail, A.S. Abousalem, G.Y. Elewady, Experimental and theoretical studies on corrosion inhibition of 4-amidinophenyl-2,2'-bifuran and its analogues in acidic media, RSC Adv. 7 (2017) 46414–46430.
[42] M.T. Alhaffar, S.A. Umoren, I.B. Obot, S.A. Ali, Isoxazolidine derivatives as corrosion inhibitors for low carbon steel in HCl solution: experimental, theoretical and effect of KI studies, RSC Adv. 8 (2018) 1764–1777.
[43] M.K. Pavithra, T.V. Venkatesha, K. Vathsals, K.O. Nayana, Synergistic effect of halide ions on improving corrosion inhibition behaviour of benzisothiozole-3-piperizine hydrochloride on mild steel in 0.5 M H_2SO_4 medium, Corros. Sci. 52 (2010) 3811–3819.
[44] P. Morales-Gil, M.S. Walczak, C. Ruiz Camargo, R.A. Cottis, J.M. Romero, R. Lindsay, Corrosion inhibition of carbon-steel with 2-mercaptobenzimidazole in hydrochloric acid, Corros. Sci. 101 (2015) 47–55.
[45] R.A. Cottis, Electrochemical methods, in: R.A. Cottis, M.J. Graham, R. Lindsay, S.B. Lyon, J.A. Richardson, J.D. Scantlebury, F.H. Stott (Eds.), Shreir's Corrosion, Corrosion in Liquids, Corrosion Evaluation, Elsevier, Amsterdam, 2010, pp. 1341–1373.
[46] M.P. Casaletto, V. Figà, A. Privitera, M. Bruno, A. Napolitano, S. Piacente, Inhibition of Cor-Ten steel corrosion by "green" extracts of *Brassica campestris*, Corros. Sci. 136 (2018) 96.
[47] Y. Zou, J. Wang, Y.Y. Zheng, Electrochemical techniques for determining corrosion rate of rusted steel in seawater, Corros. Sci. 53 (2011) 208–216.
[48] M.M. Solomon, S.A. Umoren, I.I. Udosoro, A.P. Udoh, Inhibitive and adsorption behaviour of carboxymethyl cellulose on mild steel corrosion in sulphuric acid solution, Corros. Sci. 52 (2010) 1317–1325.
[49] M.M. Solomon, H. Gerengi, S.A. Umoren, Carboxymethyl cellulose/silver nanoparticles composite: synthesis, characterization and application as a benign corrosion inhibitor for St37 steel in 15% H_2SO_4 medium, ACS Appl. Mater. Interfaces 9 (2017) 6376–6389.
[50] Mitutoyo Corporation. Surface finish analysis 2014; pp 1 – 58 (https://www.mitutoyo.com/wp-content/uploads/2012/···/1984_Surf_Roughness_PG.pd).
[51] EN ISO 4287:1998. Geometrical Product Specifications (GPS)– Surface Texture: Profile Methods – Terms, Definitions, and Surface Parameters.
[52] P.E. Alvarez, M.V. Fiori-Bimbi, A. Neske, S.A. Brandán, C.A. Gervasi, *Rollinia occidentalis* extract as green corrosion inhibitor for carbon steel in HCl solution, J. Ind. Eng. Chem. 58 (2018) 92–99.
[53] N.D. Nam, Q.V. Bui, M. Mathesh, M.Y.J. Tan, M. Forsyth, A study of 4-carboxyphenylboronic acid as a corrosion inhibitor for steel in carbon dioxide containing environments, Corros. Sci. 76 (2013) 257–266.
[54] N.D. Nam, A. Somers, M. Mathesh, M. Seter, B. Hinton, M. Forsyth, M.Y.J. Tan, The behaviour of praseodymium 4-hydroxycinnamate as an inhibitor for carbon dioxide corrosion and oxygen corrosion of steel in NaCl solutions, Corros. Sci. 80 (2014) 128–138.
[55] M.M. Solomon, H. Gerengi, S.A. Umoren, N.B. Essien, U.B. Essien, E. Kaya, Gum Arabic-silver nanoparticles composite as a green anticorrosive formulation for steel corrosion in strong acid media, Carbohydr. Polym. 181 (2018) 43–55.
[56] Y. Tang, X.P. Guo, G.A. Zhang, Corrosion behaviour of X65 carbon steel in supercritical-CO_2 containing H_2O and O_2 in carbon capture and storage (CCS) technology, Corros. Sci. 118 (2017) 118–128.
[57] M. Descostes, F. Mercier, N. Thromat, C. Beaucaire, M. Gautier-Soyer, Use of XPS in the determination of chemical environment and oxidation state of iron and sulfur samples: constitution of a data basis in binding energies for Fe and S reference compounds and applications to the evidence of surface species of an oxidized pyrite in a carbonate medium, Appl. Surf. Sci. 165 (2000) 288–302.
[58] A. Zarrouk, B. Hammouti, T. Lakhlifi, M. Traisnel, H. Vezin, F. Bentiss, New 1H-pyrrole-2,5-dione derivatives as efficient organic inhibitors of carbon steel corrosion in hydrochloric acid medium: electrochemical XPS and DFT studies, Corros. Sci. 90 (2015) 572–584.
[59] A. Moschona, N. Plesu, G. Mezei, A.G. Thomas, K.D. Demadis, Corrosion protection of carbon steel by tetraphosphonates of systematically different molecular size, Corros. Sci. 145 (2018) 135–150.
[60] W. Xu, E.H. Han, Z. Wang, Effect of tannic acid on corrosion behavior of carbon steel in NaCl solution, J. Mater. Sci. Technol. 35 (2019) 64–75.
[61] B.G. Ateya, B.E. El-Anadouli, F.M. El-Nizamy, The adsorption of thiourea on mild steel, Corros. Sci. 24 (1984) 509–515.
[62] A.A. El-Awady, B.A. Abd-El-Nabey, S.G. Aziz, Kinetic-thermodynamic and adsorption isotherms analyses for the inhibition of the acid corrosion of steel by cyclic and open-chain amines, J. Electrochem. Soc. 139 (1992) 2149–2154.
[63] S.A. Umoren, M.M. Solomon, U.M. Eduok, I.B. Obot, A.U. Israel, Inhibition of mild steel corrosion in H2SO4 solution by coconut coir dust extract obtained from different solvent systems and synergistic effect of iodide ions: ethanol and acetone extracts, J. Environ. Chem. Eng. 2 (2014) 1048–1060.
[64] E.A. Noor, A.H. Al-Moubaraki, Corrosion behavior of mild steel in hydrochloric acid solutions, Int. J. Electrochem. Sci. 3 (2008) 806–818.